From Postsynaptic Potentials to Spikes in the Genesis of Auditory Spatial Receptive Fields

José Luis Peña and Masakazu Konishi

Division of Biology, California Institute of Technology, Pasadena, California 91125

Space-specific neurons in the owl's inferior colliculus respond only to a sound coming from a particular direction, which is equivalent to a specific combination of interaural time difference (ITD) and interaural level difference (ILD). Comparison of subthreshold postsynaptic potentials (PSPs) and spike output for the same neurons showed that receptive fields measured in PSPs were much larger than those measured in spikes in both ITD and ILD dimensions. Space-specific neurons fire more spikes for a particular ITD than for its phase equivalents (ITD $\pm$ 1/F, where F is best frequency). This differential response was much less pronounced in PSPs. The two sides of pyramid-shaped ILD curves were more symmetrical in spikes than in PSPs. Furthermore, monaural stimuli that were ineffective in eliciting spikes induced subthreshold PSPs. The main cause of these changes between PSPs and spikes is thresholding. The spiking threshold did not vary with the kind of acoustic stimuli presented. However, the thresholds of sound-induced first spikes were lower than those of later sound-induced and spontaneous spikes. This change in threshold may account for the sharpening of ITD selectivity during the stimulus. Large changes in receptive fields across single neurons are not unique to the owl's space-specific neurons but occur in mammalian visual and somatosensory cortices, suggesting the existence of general principles in the formation of receptive fields in high-order neurons.

Key words: receptive fields; maps of space; sound localization; auditory system; barn owl; inferior colliculus

The receptive fields of neurons and the maps of sensory space originate primarily from topographical projections of the sensory surface. Neural systems also synthesize and map the representations of stimulus features and their combinations, as in the map of echo delays in the bat's auditory cortex and that of auditory space in the external nucleus of the inferior colliculus (ICx) in the owl (Knudsen and Konishi, 1978a; Suga et al., 1983). This type of map is referred to as a "computational map" to indicate the contrast with "projection maps" (Konishi, 1986; Knudsen et al., 1987). The cellular components of the owl's map are called space-specific neurons, because they respond only to signals coming from particular directions. These neurons receive inputs from separate pathways that process the interaural time difference (ITD) and the interaural level difference (ILD) that, respectively, define the azimuthal and elevational angles of sound sources in barn owls. Thus, the receptive field of a space-specific neuron can be defined either in real space or in terms of its tuning to ITD–ILD pairs (Peña and Konishi, 2001). These dual properties of space-specific neurons offer unique opportunities to study the cellular mechanisms for the creation of spatial receptive fields in a computational map.

Extracellular studies of space-specific neurons and the pathways leading to them have provided the basis for understanding how the owl's auditory system synthesizes the representation of auditory space (Moiseff and Konishi, 1983; Sullivan and Konishi, 1984; Takahashi et al., 1984). However, intracellular analyses are necessary for additional understanding of the processes leading to the formation of spatial receptive fields. The receptive field of a space-specific neuron consists of an excitatory center and an inhibitory surround (Knudsen and Konishi, 1978b). The exact nature of the inhibitory surround is not well understood. Space-specific neurons require binaural input. We do not know whether and how this property emerges in these cells. Space-specific neurons are selective for a single ITD. This property requires inputs from different frequency bands (Takahashi and Konishi, 1986; Mori, 1997; Mazer, 1998; Peña and Konishi, 2000), but we do not know whether this is the only requirement (Albeck and Konishi, 1995). In this article, we show how the above properties emerge after the translation of postsynaptic potentials (PSPs) to spikes in space-specific neurons.

MATERIALS AND METHODS

Data were obtained by *in vivo* intracellular recording of ICx neurons in adult barn owls. The owls were anesthetized by intramuscular injection of ketamine hydrochloride (25 mg/kg Ketaset; Phoenix Pharmaceutical, Belmont, CA) and diazepam (1.3 mg/kg; Steris Laboratories, Phoenix, AZ). An adequate level of anesthesia was maintained with supplemental injections of ketamine. The protocol for this study followed the National Institutes for Health *Guide for the Care and Use of Laboratory Animals* and was approved by the Institutional Animal Care and Use Committee of California Institute of Technology. The ICx was approached through a hole made in the exoccipital bone. We made a small hole in the bony eminence containing the optic lobe to insert the electrode.

All experiments were performed in a double-walled sound-attenuating chamber. Acoustic stimuli were digitally synthesized with a Dell (Round Rock, TX) Dimension XPS Pro200n computer and delivered by a stereo analog interface (DD1; Tucker–Davis Technologies, Gainesville, FL). ITDs were computed online, whereas two computer-controlled digital attenuators (PA4; Tucker–Davis Technologies) set ILDs. Sound stimuli, 100 msec in duration with a 5 msec linear rise/fall time, were presented once per second. Acoustic stimuli were delivered by an earphone assem-

Received Feb. 25, 2002; revised April 12, 2002; accepted April 22, 2002.

This work was supported by National Institute of Neurological Disorders and Stroke Grant DC-00134. We thank Ben Arthur for providing us with the extracellular data in the ICx; Ben Arthur, Kazuo Funabiki, Yoram Gutfreund, Eric Knudsen, Lee Moore, Teresa Nick, and Terry Takahashi for reviewing early drafts of this manuscript; and Chris Malek, Ben Arthur, and Bjorn Christianson for help with computer programming.

Correspondence should be addressed to José Luis Peña, Division of Biology 216-76, California Institute of Technology, Pasadena, CA 91125. E-mail: jose@etho.caltech.edu.

bly consisting of a Knowles Electronics (Hasca, IL) ED-1914 receiver as a sound source, a Knowles BF-1743 damped coupling assembly for smoothing the frequency response of the receiver, and a calibrated Knowles 1939 microphone for monitoring sound pressure levels in the ear canal. The Knowles components were encased in an aluminum cylinder that was 7 mm in diameter and 8.1 mm in length. The cylinder was inserted into the ear, and the gaps between the earphone assembly and the ear canal were sealed with silicone impression material (Gold Velvet; All American Laboratories, Oklahoma City, OK). The calibration data contained the amplitudes and phase angles measured in steps of 100 Hz. Irregularities in the frequency response of each earphone were automatically smoothed by the computer from 2 to12 kHz.

Sharp borosilicate glass electrodes filled with 2 M potassium acetate and 4% neurobiotin were used for intracellular recording of space-specific neurons. Analog signals were amplified (Axoclamp 2A; Axon Instruments, Foster City, CA) and stored in the computer. We identified ICx neurons by labeling their axons, which project to the optic tectum. The tracer neurobiotin was injected by iontophoresis (3 nA positive, 300 msec current steps; three per second for 5–30 min). After the experiment, the owls were overdosed with Nembutal and perfused with 2% paraformaldehyde. Brain tissue was cut in 60-μm-thick sections and processed according to standard protocols (Kita and Armstrong, 1991).

We computed the median of membrane potentials during the first 50 msec of the response to sound (Peña and Konishi, 2001). We then calculated mean membrane potentials by averaging median potentials over five stimulus presentations. Mean resting potentials are the means of median membrane potentials averaged over all trials within a period of 100 msec before each stimulus onset. ITD and intensity response curves of PSPs were made by custom software written in Matlab 6 (MathWorks, Natick, MA).

The width of ITD and ILD curves differed between spike and membrane potential data. We used two different criteria for the sharpness of these curves. One was the width at half-height (50% of the difference between the maximal and minimal responses measured in spikes or PSPs). The other was a tuning ratio, $(R_{max} - R_{min})/\text{sum}(R_i - R_{min})$. R_{max} is the mean maximal spike rate or maximal membrane depolarization, corresponding to the main ITD peak and ILD peak, and R_{min} is the mean minimal spike rate or the mean maximal hyperpolarization, corresponding to the trough next to the main ITD peak and the bottom of pyramid-shaped ILD curves. R_i is the mean spike rate or membrane potential for the sampled ITD or ILD.

The symmetry of ILD curves differed between spike and membrane data. We represent the degree of symmetry by $\text{sum}(R_{contra} - R_{ipsi})^2$, which compares the area below the curve between the two sides of the peak. R_{contra} and R_{ipsi} are the mean spike rates or membrane potentials at the same ILD intervals for the contralateral and ipsilateral sides of the peak. The number of spikes and membrane potential values were normalized to the maximal-to-minimal range. Neurons with a best ILD that was within ±10 dB were used for this analysis.

The spiking threshold was automatically measured by a modified version of the method used by Azouz and Gray (1999). The threshold corresponded to the membrane potential at the onset of the spike at which the first derivative (dV/dt) was equal to a fraction of its maximum. The fraction of the first derivative that we chose was 0.1 after visual inspection of the computed threshold for a range of fractions from 0 to 0.3 in spikes of all the neurons. Spikes were detected by a minimum first derivative of 72 mV/msec together with a positive second derivative. This double requirement made the algorithm robust in detecting only spikes and avoiding smaller and fast membrane potential deflections. The data were interpolated at five times the original sampling rate (24 kHz). Thresholds were normalized to the difference from resting potential for each neuron. Mean spike rates were derived from five repetitions of each stimulus. Spontaneous spike rates were measured during the 100 msec period before the stimulus onset.

The rate of depolarization preceding spikes was computed as the mean of the first derivative during the 2 msec period before the beginning of the spike. Spike thresholds and depolarization rates were better correlated during this period than during later periods. Only the spikes that were not preceded by other spikes in the previous 10 msec interval were included. A minimum of 10 events was used to calculate the mean rate of depolarization for spontaneous spikes.

RESULTS

The data came from intracellular recordings of 75 neurons in the external nucleus of the ICx in 24 owls. We used neurobiotin to label 25 of the 75 neurons to determine the sites of their axon terminals. We could trace the axons to the optic tectum in 15 of the 25 labeled neurons, indicating that they are ICx cells. All 75 neurons responded selectively to combinations of ITD and ILD. This and other physiological properties, such as broad frequency tuning and a preference for a particular ITD, showed that all of these neurons belong to the ICx. Mean impulse rates or amplitudes of PSPs plotted against ITD and ILD are referred to as ITD and ILD curves, respectively (Fig. 1). In making an ITD or an ILD curve, we paired the best ILD with all sample ITDs that varied in steps of 30 μsec and the best ITD with all sample ILDs that varied in steps of 5 dB, respectively.

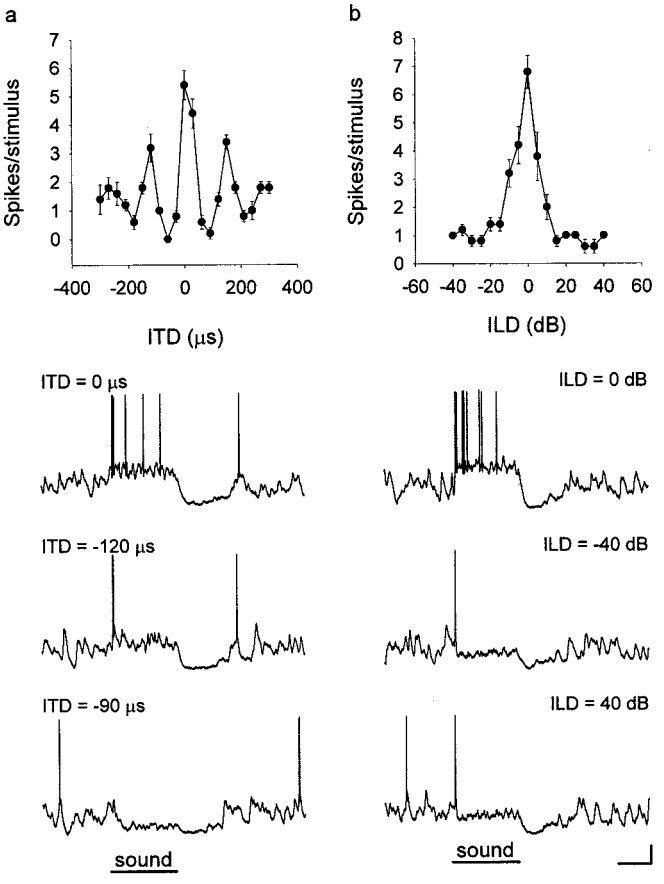

Figure 1. ITD and ILD tuning. ICx neurons are tuned to combinations of ITD and ILD. The ITD (*a*) or ILD (*b*) curve of a neuron is obtained by presenting different values of one cue while the most favorable value of the other cue is held constant. Sample intracellular traces show how the same neuron responded to different combinations of ITD and ILD. Values of ITD and ILD are shown *above* each trace. Error bars indicate SEM over five trials of each stimulus. Calibration: 10 mV, 50 msec.

We selected neurons according to the following set of criteria: the stability of recording during the period of data acquisition (which varied from 15 min to >1 hr), resting potentials of more than −50 mV (mean resting membrane potential of the 75 neurons was −67.6 ± 9.3 mV), and action potential amplitudes of >40 mV from threshold (Fig. 1). We also compared the firing rate of the neurons used in this study with data from 95 extracellularly recorded ICx neurons (courtesy of Ben Arthur, California Institute of Technology, Pasadena, CA). The mean spontaneous rate of the extracellularly recorded neurons (2.2 ± 3.3 spikes/sec) was not significantly different from that of the intracellularly recorded neurons (3.1 ± 6.7 spikes/sec). The width of the main ITD peak

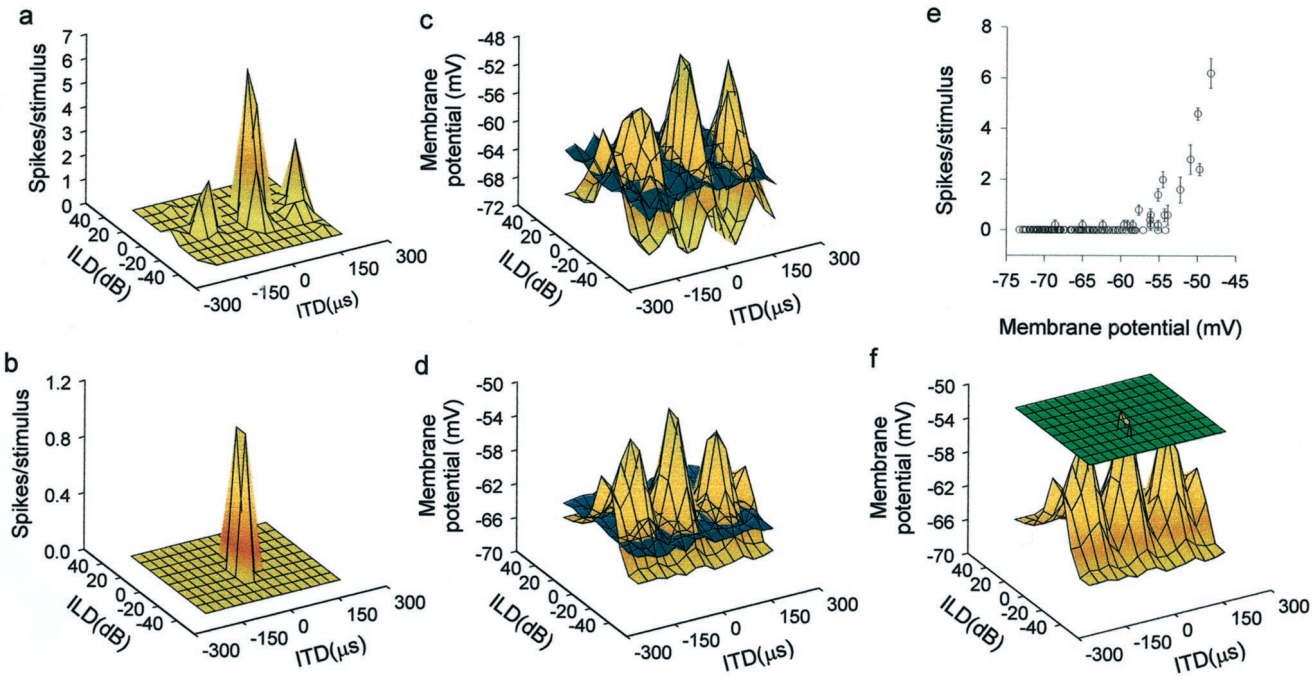

Figure 2. Transformations in auditory spatial receptive fields. Receptive fields measured by spiking rate showed either a single tall peak (*b*) or one tall (main) peak plus smaller side peaks, as in most neurons (*a*). However, the receptive fields (*brown* surfaces) measured in subthreshold PSPs had multiple peaks of similar amplitude surrounded by areas of hyperpolarization below the resting potential (*blue* surfaces) (*c, d*). This difference is partly because of a mechanism that converts small differences in membrane potentials to large changes in spike rates (*e*). In addition, thresholding (*green* surface represents mean spike threshold measured from membrane potential records) greatly contributes to the isolation of the main peak from other peaks (*f*). Data in each *row* came from the same neuron.

of the extracellularly recorded neurons (55.3 ± 14.5 μsec) was slightly but significantly broader than that of the intracellularly recorded neurons (50.8 ± 8.18 μsec; *t* test; $p = 0.020$). The widths of ILD curves in the extracellular data (19.0 ± 8.1 dB) and intracellular data (21.1 ± 9.2 dB) were not significantly different. Also, the temporal pattern of discharge as judged by peristimulus time histograms was not different between the two groups (data not shown). These comparisons show that intracellular recording did not significantly alter the response properties of ICx neurons.

Plots of membrane potential as a function of ITD and ILD usually show peaks of depolarization surrounded by areas of subthreshold membrane potentials, including IPSPs (Fig. 2). All of the neurons we studied showed this phenomenon, which is basically consistent with the excitatory center and inhibitory surround organization of receptive fields found in an extracellular free-field study (Knudsen and Konishi, 1978b). Note the differences in the receptive field size and structure between spike rate and membrane potential data (Fig. 2, *a* vs *c* and *b* vs *d*). Below, we elaborate on these differences for the ITD and ILD aspects of receptive fields separately.

Tuning to ITD

Space-specific neurons respond to an ITDi (i stands for frequency independent) and its phase equivalents, ITDi ± T, where T is the inverse of their best frequency (BF) (T = 1/BF). This relationship means that neurons can have more than one ITD peak. When the stimulus is broadband, the spike output of space-specific neurons usually shows a tall main peak at ITDi and shorter or no "side peaks" at ITDi ± T. In contrast, plots of membrane potential and ITD showed multiple peaks in which the main peak was only slightly higher than the side peaks. These differences between subthreshold and spike data are attributable to thresholding. The spiking threshold may be just below the tip of the main peak but above those of the side peaks to produce an ITD curve with one peak, as in the example shown in Figure 2*b*. When the threshold is well below the tip of the main peak and slightly below the tips of the side peaks, an ITD curve with a large main peak and smaller side peaks results, as in most neurons (Fig. 2*a*).

Along the ITD axis, a large trough occurred on both sides of the main peak (Fig. 3*a*). The ITDs that caused these deep troughs were half-period (1/2T) from ITDi. For example, if a neuron with best frequency of 5 kHz (i.e., period = 200 μsec) has its main ITD peak at 30 μsec, representing a contralateral site, a deep trough occurs at 130 μsec (= 30 + 100) on the same side and at −70 μsec (= 30 − 100) on the other side. When the stimulus was a broadband noise, combinations of ITDi ± 1/2T with any ILD induced IPSPs. In contrast, combinations of ITDs corresponding to the outside troughs of the first side peaks (i.e., ITDi ± 1.5T) and the best ILD did not induce hyperpolarization with broadband signals.

The ITD tuning of subthreshold potentials was broader than that of spike rates. The tuning to ITD can be represented by either the width of the main peak at half-height or the ratio between the response to best ITD and the response to all sampled ITDs under the tuning curve (tuning ratio; see Materials and Methods). Whereas the width measures the tuning of a restricted area around the best ITD, the tuning ratio includes all responses under the curve. Here, a large width and a small ratio mean broad tuning. The main ITD peak was significantly broader for PSPs (75.17 ± 17.12 μsec) than for the spike rate (50.82 ± 8.18 μsec; paired *t* test; $p < 0.0001$) (Fig. 4*a*). Similarly, the tuning ratio was significantly smaller for PSPs (0.09 ± 0.02) than for the spike rate (0.23 ± 0.17; paired *t* test; $p < 0.0001$) (Fig. 4*b*).

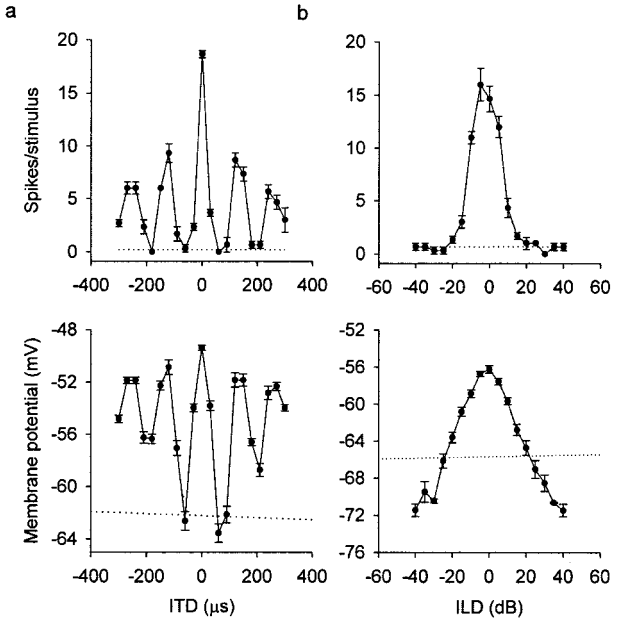

Figure 3. Changes in ITD and ILD tuning. *a*, ITD curves of spike rates show one large main peak in spike rate (*top*), whereas PSPs show side peaks and areas of hyperpolarization flanking the main peak (*bottom*). *b*, ILD curves are narrow and pyramid-shaped in spike rate (*top*) and broader in PSPs (*bottom*) for the same neuron. Error bars indicate SEM. *Dotted lines* represent the mean spontaneous discharge or mean resting potential.

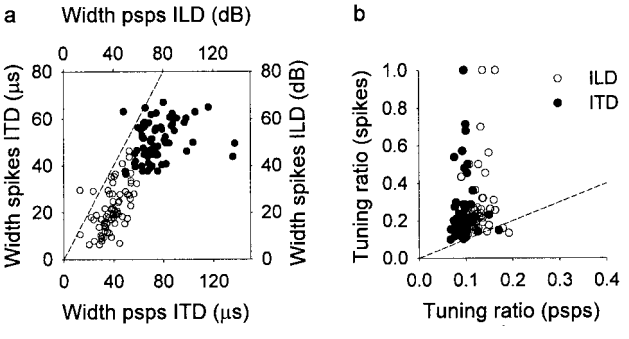

Figure 4. Sharpening of ITD and ILD tuning. This figure shows, for each neuron, the ITD and ILD tuning width and tuning ratio measured in PSPs and spike rates. *a*, The width of the main peak of ITD (*filled circles*) and ILD (*open circles*) tuning curves is narrower in spike rates than in PSPs. *b*, For both ITD (*filled circles*) and ILD (*open circles*), the tuning ratio in spike rates is significantly larger (i.e., narrower tuning) than in PSPs. The *dashed line* in each *panel* would result if the tuning width or ratio were the same for spike rates and PSPs.

Tuning to ILD

All of the space-specific neurons of this sample had pyramid-shaped ILD curves in terms of spike rates. The ILD tuning curves of subthreshold potentials were much broader than those of spike rates (Fig. 3*b*). ILD curves were significantly broader for PSPs (38.65 ± 10.07 dB) than for spikes (21.10 ± 9.24 dB; paired *t* test; $p < 0.0001$) (Fig. 4*a*). Similarly, the tuning ratios of ILD curves were significantly smaller for PSPs (0.12 ± 0.02) than for spike rates (0.26 ± 0.18; paired *t* test; $p < 0.0001$) (Fig. 4*b*). This difference was attributable partly to thresholding, which takes only the top portion of ILD-tuned PSPs. Another nonlinear process contributes to the difference in tuning ratios by converting small differences in suprathreshold membrane potentials into large changes in the firing rate (Fig. 2*e,f*).

Another conspicuous difference between subthreshold and spike data concerns the symmetry of ILD curves. In 32 of 55 neurons, ILD curves of PSPs were pyramid-shaped. In these neurons, large ILDs paired with any ITD induced IPSPs on both sides of the pyramid. For example, either +40 dB (+ means louder in contralateral ear) or −40 dB (louder in ipsilateral ear) paired with any ITD induced IPSPs (the segment of the pyramid extending below the resting membrane potential) (Fig. 3*b*). In the remaining 23 neurons, ILD curves for PSPs were not completely pyramid-shaped but were asymmetrical, with one slope of the pyramid being less steep than the other. When one side of the ILD curves was more depolarized, a large ILD favoring that side (i.e., louder), paired with any ITD, depolarized the neuron to a subthreshold level, whereas a large ILD favoring the other side, paired with any ITD, hyperpolarized the cell (Fig. 5*b*). Asymmetrical slopes were independent of the sign of ILD (louder or weaker in one ear) and occurred on either the ipsilateral ($n = 11$) or contralateral ($n = 12$) side of the recording site. In contrast to the ILD curves of subthreshold potentials, those of spikes in our sample showed little asymmetry (Fig. 5*a*). The symmetry of ILD curves was quantified by comparing the difference in area below each side of the peak (see Materials and Methods). ILD curves for PSPs showed a significantly larger degree of asymmetry than those for spikes (paired *t* test; $p < 0.0001$) (Fig. 5*c*). Thus, the spiking threshold tended to be above the shoulder of the less steep slope of the curves.

Translation from membrane potential to spikes

Thresholding appears to play a major role in the formation of receptive fields. To determine whether the spiking threshold changes for different kinds of stimuli, we measured the spiking threshold during acoustic signals that evoked PSPs of different amplitudes. We measured the spiking threshold in all 75 neurons (Fig. 6*a*). The mean threshold of the first spike (onset spike) after the stimulus onset was −53.5 ± 10.4 mV. Changes in threshold to more depolarized or hyperpolarized levels are defined as threshold increases and decreases, respectively. The spike threshold varies with slowly changing membrane potential. To compensate for this variation in threshold, we subtracted individual thresholds from the resting potential for each neuron (Fig. 6*c*). The mean threshold could increase in each neuron by as much as 10 mV when the discharge rate increased. The threshold of spiking increased as interspike intervals decreased and increased with the number of preceding spikes during evoked responses (data not shown). The threshold of the onset spike was significantly lower than the rest (paired *t* test; $p < 0.004$). A reduction in the available number of sodium channels may be the cause of these phenomena through voltage-dependent inactivation.

The stimulus-induced first spike showed a lower threshold than both the spikes that followed it and spontaneous spikes (Fig. 6*a*, *arrow*). The difference between the mean threshold of the onset spike and of spontaneous spikes was statistically significant in the group of neurons that showed measurable spontaneous activity ($n = 52$; paired *t* test; $p < 0.0001$).

The spike threshold was inversely correlated with the preceding rate of membrane depolarization (Fig. 6*b*). For a subset of 20 neurons with firing rates exceeding one spike per stimulus and with spontaneous discharge, we normalized both the thresholds and the preceding depolarization rate so that we could compare different neurons. Higher thresholds (the difference between

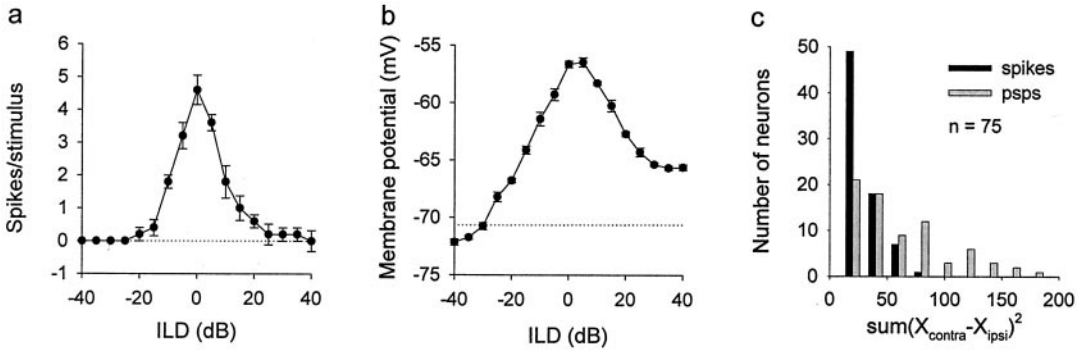

Figure 5. Symmetry and asymmetry in ILD curves. ILD curves measured in spikes (*a*) tend to be more symmetrical than their respective PSP curves (*b*). Error bars indicate SEM. *Dotted lines* represent the mean spontaneous discharge or mean resting potential. *c*, Distribution of symmetry indices for spikes and PSPs.

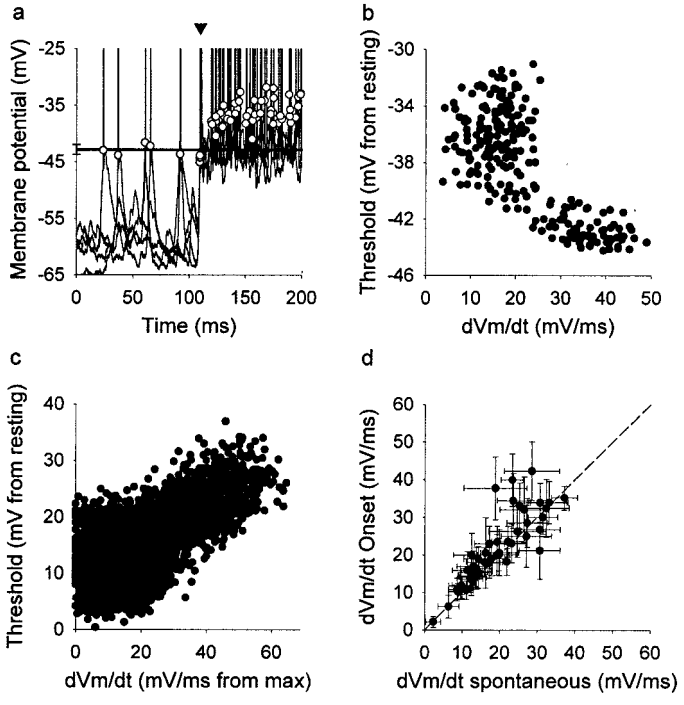

Figure 6. Spiking threshold. *a*, Automatic computation of thresholds in four overlaid traces from a single neuron. *Circles* indicate the threshold for each spike. The *arrowhead* indicates the onset spikes in the response induced by sound. The thresholds of all onset spikes fall below the mean threshold of spontaneous spikes (*solid line*). Sound stimulation starts at 100 msec. *b*, Plot of the spike threshold versus the rate of depolarization (dVm/dt) of the same neuron as in *a*. The threshold is lower when the rate of the preceding depolarization is steeper. *c*, The rate of depolarization is inversely correlated with the spike threshold in a subset of 20 neurons. The threshold decreases (moves closer to the resting potential) when the rate of depolarization that precedes the spikes increases (gets closer to the maximum rate). *d*, In most neurons (45 of 52 neurons), the rate of depolarization preceding the onset spike evoked by sound shows higher values than for spontaneous spikes. Error bars indicate SEM. The *dashed line* would result if the rate of depolarization were the same for spontaneous and sound induced spikes.

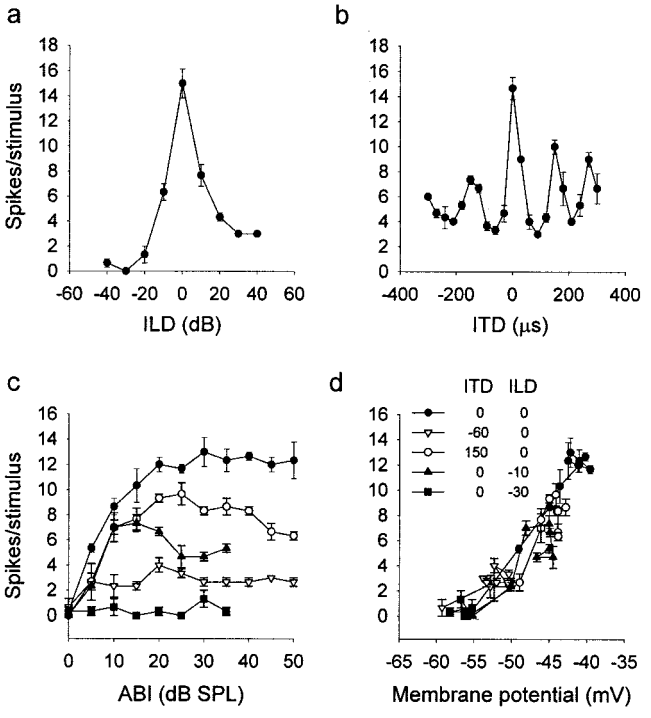

Figure 7. Spike threshold is independent of stimuli. *a*, ILD curve. *b*, ITD curve from the same neuron. *c*, Rate–intensity curves for different stimuli indicated by different symbols. *d*, Number of spikes versus membrane potential evoked by sound. The response to different combinations of ITD and ILD at different sound levels shows similar trends, indicating that for the same membrane potential, the cell will respond with a similar number of spikes despite differences in stimuli. *ABI*, Average binaural intensity; *SPL*, sound pressure level.

threshold and resting potential increased) were correlated with smaller depolarization rates (larger differences between the depolarizing rate and its maximum) (Fig. 6). In addition, the mean depolarizing rate of spontaneous spikes was significantly smaller than that of the spikes evoked by the stimulus onset (paired *t* test; $p < 0.001$; $n = 52$) (Fig. 6*d*).

There is evidence in support of the modulation of the spike threshold by the synaptic input (Cantrell and Catterall, 2001). We studied whether PSPs with similar mean membrane potential evoked by different sounds were translated into the same number of spikes. In the ICx, similar levels of depolarization can be obtained by adjusting sound level for different pairs of ITDs and ILDs. We found that the neurons tended to translate the same mean membrane potential into the same number of spikes independently of the stimulus ($n = 5$) (Fig. 7). Thus, the spiking threshold or the mechanism involved in spike generation is not dynamically adjusted for the processing of particular ITD–ILD pairs.

DISCUSSION

Excitatory center and inhibitory surround organization

Using the methods of free-field stimulus presentation and extracellular recording, Knudsen and Konishi (1978b) found that the receptive field of a space-specific neuron consisted of an excitatory center and an inhibitory surround. To study the extent of the inhibitory surround, they placed one speaker in the excitatory center and moved a second speaker around it. Our intracellular data were consistent with the results of the free-field study except for the properties of inhibitory surrounds. The free-field study reported that inhibition was stronger in the immediate vicinity of the excitatory center than in areas farther out. This phenomenon is attributable to the large hyperpolarization flanking the main ITD peak. The gradual loss of inhibitory strength with distance from the main ITD peak is attributable to the depolarization corresponding to the first side peaks. The free-field study did not find a similar gradient of inhibition in elevation, although stimuli coming from below or above the excitatory center reduced spike rates. This contrast is partly because the elevational dimension of receptive fields is longer than the azimuthal, and because the slopes of the ILD peak taper off less steeply than those of the ITD. The present study shows that inhibitory hyperpolarizations increase instead of decrease as ILD departs from its best value.

The inhibitory surrounds as mapped by the free-field methods were large, usually covering the entire frontal field (+60° to −90° in elevation ± 60° in azimuth) and sometimes extending to the back of the head. These findings are consistent with the intracellular findings; both ITD and ILD values that departed far from their best values induced either hyperpolarizations or subthreshold depolarizations. All space-specific neurons in the present study produced either hyperpolarizations or subthreshold responses to broadband monaural stimuli, which are large ILD outside the normal range of this cue. These findings indicate that the inhibitory surrounds of space-specific neurons, as studied with broadband signals, have no outer boundaries. This property may be unique to receptive fields created by computation. Even the influence of stimuli located well outside the classical receptive field in the visual cortex is spatially limited (Allman et al., 1985).

Input–output transformations

The nature of input–output transformations can be inferred from the anatomical connections and physiological differences between the recorded neuron and its afferents. In addition, the relationships between PSPs and the stimuli that induced them reveal the nature of the input to the recorded neuron. The generation of spikes constitutes the final stage of input–output conversion. The results presented above show that large and important changes occur in the stimulus-response relationships across space-specific neurons.

ICx, where space-specific neurons reside, receives input from the ipsilateral lateral shell of the central nucleus of the ICx (LS). The subthreshold responses of space-specific neurons reflect both the properties of LS neurons and the relationships between the LS and the ICx. Frequency tuning is narrower, and the difference between the main ITD and side peaks is smaller in the LS than in the ICx (Gold and Knudsen, 2000). LS neurons tuned to different frequencies converge on single ICx neurons (Wagner et al., 1987). This frequency convergence partly contributes to the increase in the relative amplitude of the main ITD peak over the side peaks in ICx neurons (Takahashi and Konishi, 1986; Peña and Konishi, 2000). Although the resolution of phase ambiguity requires frequency convergence, it is thresholding that enhances the dominance of the main ITD peak.

LS neurons are sensitive to ITD and ILD, but their ILD curves may show varying degrees of asymmetry, including sensitivity to large ILDs and monaural stimuli (Adolphs, 1993). Consistent with this broad ILD tuning is the fact that ILD selectivity does not vary systematically in the LS, in contrast to the ICx, where it shows ordered shifts in the axis orthogonal to the ITD coordinate (Brainard and Knudsen, 1993). Approximately one-half of the space-specific neurons we examined had asymmetrical ILD curves in their subthreshold responses. Although this asymmetry may be relevant for the sensitivity of some space-specific neurons to the direction of stimulus movement, the output of these same neurons showed little asymmetry in their ILD response to motionless spatial cues. In summary, thresholding plays a crucial role in the formation of major properties of space-specific neurons, including their sharp ITD and ILD tuning, large difference between the main and side ITD peaks, and exclusively binaural responses.

Thresholding may also be involved in the changes in ITD and ILD tuning during stimulation. Spike rate ITD and ILD curves sharpen with time during stimulation (Wagner, 1990). This phenomenon may originate in the process of conversion from membrane potentials to spikes. The fast depolarization rate at the beginning of the response more easily triggers spikes, broadening the tuning to ITD and ILD at the response onset. The tuning then increases as the spike threshold rises after the stimulus onset. The mechanisms involved may be the inactivation of Na^+ channels by the sustained depolarization and the lower depolarization rates that precede the spikes. Although the spike thresholds we measured and depolarization rates are correlated, the available data cannot completely rule out the possibility that recorded and actual spike thresholds are different and dissociated. We assume that we are recording at or near the neuronal soma, but we cannot exactly determine the electrode location relative to the spike-initiating site and how the changes in membrane potential in both compartments are interrelated.

What regulates the spiking threshold *in vivo* is not well understood. Synaptic inputs may influence the spiking threshold by modulation of voltage-gated Na^+ channels (Cantrell and Catterall, 2001). In the owl's space-specific neurons, the spiking threshold changes with firing rate and interspike interval. However, these variations are not correlated with the processing of particular stimulus properties, because similar levels of depolarization evoke similar numbers of spikes independently of what ITDs and ILDs are involved. The spike threshold is also affected by the rate of depolarization of the membrane potential in visual cortex neurons, allowing the system to detect synchronous synaptic inputs (Azouz and Gray, 2000). The steeper onset of the EPSPs generated by acoustic signals triggers spikes more effectively than spontaneous EPSPs. This change in the shape of PSPs may represent a switch that allows the system to operate in a spontaneous or an evoked mode with different sensitivity.

The response of space-specific neurons represents the results of all computations that take place in the parallel and hierarchically organized pathways leading to the ICx. Major steps such as the detection and mapping of ITDs and ILDs occur in lower-order stations (Manley et al., 1988; Carr and Konishi, 1990; Takahashi and Keller, 1992; Adolphs, 1993; Mogdans and Knudsen, 1994; Peña et al., 2001). However, the results of these processes are insufficient for encoding auditory space, because they contain ambiguities such as the inability to discriminate between an ITD

and its phase equivalents and between monaural and binaural stimuli. These ambiguities disappear across space-specific neurons. Thus, large changes occur at the final level of synthesizing the representation of auditory space.

The types of transformation found in space-specific neurons are not unique to the owl's auditory system. The dimensions and other properties of receptive fields in the visual and somatosensory cortices show large differences between the PSPs and the spike output of a neuron (Ferster and Jagadeesh, 1992; Frégnac et al., 1996; Li and Waters, 1996; Bringuier et al., 1999; Carandini and Ferster, 2000; Volgushev et al., 2000). Receptive field sizes measured by membrane potentials are much larger than those measured by spike rates. Thresholding is a major means by which visual cortical cells reduce the size of receptive fields measured in PSPs (Carandini and Ferster, 2000; Volgushev et al., 2000). These similarities between different sensory systems in various animal species suggest similar designs and methods of creating receptive fields in high-order neurons.

REFERENCES

Adolphs R (1993) Bilateral inhibition generates neuronal responses tuned to interaural level differences in the auditory brain stem of the barn owl. J Neurosci 13:3647–3668.

Albeck Y, Konishi M (1995) Responses of neurons in the auditory pathway of the barn owl to partially correlated binaural signals. J Neurophysiol 74:1689–1700.

Allman J, Miezin F, McGuinness E (1985) Stimulus specific responses from beyond the classical receptive field: neurophysiological mechanisms for local-global comparisons in visual neurons. Annu Rev Neurosci 8:407–430.

Azouz R, Gray CM (1999) Cellular mechanisms contributing to response variability of cortical neurons *in vivo*. J Neurosci 19:2209–2223.

Azouz R, Gray CM (2000) Dynamic spike threshold reveals a mechanism for synaptic coincidence detection in cortical neurons in vivo. Proc Natl Acad Sci USA 97:8110–8115.

Brainard MS, Knudsen EI (1993) Experience-dependent plasticity in the inferior colliculus: a site for visual calibration of the neural representation of auditory space in the barn owl. J Neurosci 13:4589–4608.

Bringuier V, Chavane F, Glaeser L, Frégnac Y (1999) Horizontal propagation of visual activity in the synaptic integration field of area 17 neurons. Science 283:695–699.

Cantrell AR, Catterall WA (2001) Neuromodulation of Na^+ channels: an unexpected form of cellular plasticity. Nat Rev Neurosci 2:397–407.

Carandini M, Ferster D (2000) Membrane potential and firing rate in cat primary visual cortex. J Neurosci 20:470–484.

Carr CE, Konishi M (1990) A circuit for detection of interaural time differences in the brain stem of the barn owl. J Neurosci 10:3227–3246.

Ferster D, Jagadeesh B (1992) EPSP-IPSP interactions in the cat visual cortex studied with *in vivo* whole-cell patch recording. J Neurosci 12:1262–1274.

Frégnac Y, Bringuier V, Chavane F, Glaeser L, Lorenceau J (1996) An intracellular study of space and time representation in primary visual cortical receptive fields. J Physiol (Paris) 90:189–197.

Gold JI, Knudsen EI (2000) A site of auditory experience-dependent plasticity in the neural representation of auditory space in the barn owl's inferior colliculus. J Neurosci 20:3469–3486.

Kita H, Armstrong W (1991) A biotin-containing compound *N*-(2-aminoethyl) biotinamide for intracellular labeling and neuronal tracing studies: comparison with biocytin. J Neurosci Methods 37:141–150.

Knudsen EI, Konishi M (1978a) A neural map of auditory space in the owl. Science 200:795–797.

Knudsen EI, Konishi M (1978b) Center-surround organization of auditory receptive fields in the owl. Science 202:778–780.

Knudsen EI, Du Lac S, Esterly SD (1987) Computational maps in the brain. Annu Rev Neurosci 10:41–65.

Konishi M (1986) Centrally synthesized maps of sensory space. Trends Neurosci 9:163–168.

Li CX, Waters RS (1996) In vivo intracellular recording and labeling of neurons in the forepaw barrel subfield (FBS) of rat somatosensory cortex: possible physiological and morphological substrates for reorganization. NeuroReport 7:2261–2272.

Manley GA, Köppl C, Konishi M (1988) A neural map of interaural intensity differences in the brainstem of the barn owl. J Neurosci 8:2665–2676.

Mazer J (1998) How the owl resolves auditory coding ambiguity. Proc Natl Acad Sci USA 95:10932–10937.

Mogdans J, Knudsen EI (1994) Representation of interaural level difference in the VLVp, the first site of binaural comparison in the barn owl auditory-system. Hear Res 74:148–164.

Moiseff A, Konishi M (1983) Binaural characteristics of units in the owl's brainstem auditory pathway: precursors of restricted spatial receptive fields. J Neurosci 3:2553–2562.

Mori K (1997) Across-frequency nonlinear inhibition by GABA in processing of interaural time difference. Hear Res 111:17–30.

Peña JL, Konishi M (2000) Cellular mechanisms for resolving phase ambiguity in the owl's inferior colliculus. Proc Natl Acad Sci USA 97:11787–11792.

Peña JL, Konishi M (2001) Auditory spatial receptive fields created by multiplication. Science 292:249–252.

Peña JL, Viete S, Funabiki K, Saberi K, Konishi M (2001) Cochlear and neural delays for coincidence detection in owls. J Neurosci 21:9455–9459.

Suga N, Oneil WE, Kujirai K, Manabe T (1983) Specificity of combination-sensitive neurons for processing of complex biosonar signals in auditory-cortex of the mustached bat. J Neurophysiol 49:1573–1626.

Sullivan WE, Konishi M (1984) Segregation of stimulus phase and intensity coding in the cochlear nucleus of the owl. J Neurosci 4:1787–1799.

Takahashi TT, Keller CH (1992) Commisural connections mediate inhibition for the computation of interaural level difference in the barn owl. J Comp Physiol [A] 170:161–169.

Takahashi TT, Konishi M (1986) Selectivity for interaural time difference in the owl's midbrain. J Neurosci 6:3413–3422.

Takahashi TT, Moiseff A, Konishi M (1984) Time and intensity cues are processed independently in the auditory system of the owl. J Neurosci 4:1781–1786.

Volgushev M, Pernberg J, Eysel UT (2000) Comparison of the selectivity of postsynaptic potentials and spike responses in cat visual cortex. Eur J Neurosci 12:257–263.

Wagner H (1990) Receptive fields of neurons in the owl's auditory brainstem change dynamically. Eur J Neurosci 2:949–959.

Wagner H, Takahashi TT, Konishi M (1987) Representation of interaural time difference in the central nucleus of the barn owl's inferior colliculus. J Neurosci 7:3105–3116.